ACS OMEGA

Open Access

http://pubs.acs.org/journal/acsodf

Article

Investigation of the Nonionic Acidizing Retarder AAO for Reservoir Stimulation

Zhonghao Chen, Hongping Quan,* Zhiyu Huang,* and Yang Wu

Cite This: *ACS Omega* 2023, 8, 39041−39051

Read Online

ACCESS | Metrics & More | Article Recommendations

ABSTRACT: In the process of matrix acidizing, reducing the reaction rate between hydrochloric acid and carbonate rock to increase oil and gas production has become one of the biggest challenges in reservoir stimulation. An adsorption film formed on rocks can effectively postpone the contact between the hydrogen ion and rock, which is of great significance in decreasing the rate of an acid−rock reaction. In this study, nonionic acidizing retarder AAO was synthesized by acrylamide, allyl poly(ethylene glycol), and octadecyl methacrylate. The structure of AAO was characterized by Fourier transform infrared (FT-IR) spectrometry and ^{1}H nuclear magnetic resonance (^{1}H NMR). The reaction of AAO retard acid and 20% hydrochloric acid with $CaCO_3$ was studied at 50 °C, and the amount of CO_2 generated at different times was recorded. The etching time of 0.8% AAO retard acid to $CaCO_3$ could be up to 120 min, whereas 20% hydrochloric acid (without AAO) ended at 45 min, which showed that AAO had the potential to defer the acid−rock reaction. The adsorption behavior of AAO on $CaCO_3$ matched the pseudo-second-order kinetic model well. Meanwhile, the addition of urea greatly reduced the adsorption amount of AAO on $CaCO_3$, which showed that the hydrogen bond was the driving force for the adsorption process. Additionally, the results of X-ray photoelectron spectroscopy (XPS) showed that the N element from acrylamide appeared on the surface of $CaCO_3$ after adsorption. Scanning electron microscopy (SEM) demonstrated that a smooth and dense thin film existed on the surface of $CaCO_3$ treated with AAO retard acid. The change in the vibration peak of C═O from 1720 to 1650 cm^{-1} indicated that the ester groups in AAO had been hydrolyzed, which was beneficial to film desorption and the reduction of reservoir damage. Therefore, this paper could help with research on carbonate acidizing for reservoir stimulation.

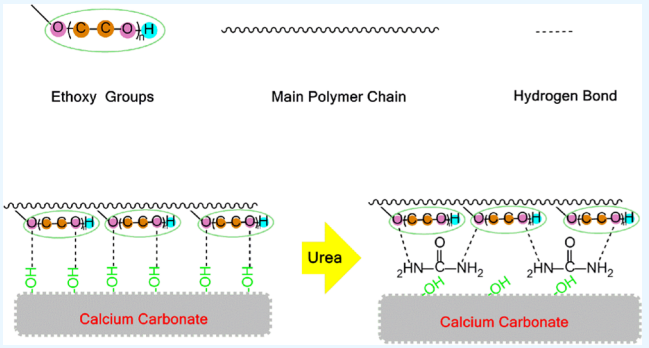

1. INTRODUCTION

Energy demand for nonrenewable energy sources such as oil and natural gas increases with the rapid development of the global industry. Worldwide, more than 50% of crude oil comes from carbonate reservoirs[1,2] and $CaCO_3$ is the main component of carbonate reservoirs, but the recovery rate of primary and secondary crude oil is below 45%.[3,4] As a commonly used method for reservoir stimulation, acidizing operations can significantly improve oil and gas production.[5] According to the different operation processes, acidizing can be divided into three types: pickling, matrix acidizing, and acid fracturing.[6] Matrix acidizing aims to dissolve blockages in the pore channel with acid solution under the condition below formation fracture pressure, thereby increasing formation permeability. Due to the low construction pressure, effective cracks cannot be formed by fracturing the formation, so it can only be constructed in the near well area. However, in the process of matrix acidizing, the reaction rate between hydrochloric acid and $CaCO_3$ is too fast, resulting in the poor stimulation of oil and gas wells.[7] For carbonate rocks, matrix acidizing will also form a dissolution pore with many small branches. The treatment by retarding acid can add more small branches for the free flow of oil and gas, which is of great significance for improving oil and gas production. Mustafa et al. reported a new type of green and efficient acid system and revealed its acid etching efficiency by measuring its reactivity with three types of rocks (Austin Chalk, Indiana Limestone, and Silurian Dolomite). The results showed that the acid etching efficiency is chalk, limestone, and dolomite in descending order.[8] When using hydrochloric (HCl) or acetic (HAc) acid in matrix acidizing, the higher the degree of dolomitization of the carbonate rocks, the lower the rate of dissolution. For the carbonate outcrops with low dolomite contents, there will be produced a smooth surface when

Received: May 31, 2023
Accepted: September 22, 2023
Published: October 11, 2023

https://doi.org/10.1021/acsomega.3c03849
ACS Omega 2023, 8, 39041−39051

reacting with HCl, while a rough surface will be observed when reacting with HAc.[9] In addition, Mehrjoo et al. hold this view that a high concentration of HCl (15%) is suitable for calcite-dominated carbonate reservoirs, while HCl solution (7%) can significantly improve fracture conductivity for dolomite.[10] The experimental results conducted by Martyushev et al. also confirmed that the content of calcite and dolomite in carbonate reservoirs has an enormous effect on the efficiency of acid fracturing, and the optimal acid injection rate needs to be considered.[11] Presently, the acidizing systems primarily comprise gelled acid, emulsified acid, foamed acid, and self-diverting acid.[12,13] Although the gelled acid with high viscosity can considerably delay the migration of H^+ and reduce the reaction rate, incomplete flowback frequently occurs due to the molecular hydrodynamic volume being larger than the pore throat radius of the reservoir.[14] Seriously, the filter cake can form to block the pores.[15] The stability of emulsified acid and foamed acid at high temperatures plagues its extensive applications. The above methods all reduce the reaction rate by controlling the transport of H^+. However, because of the characteristics of fluid and rock, adsorption occurs frequently during formation reconstruction.[16−18]

The reaction of an acid solution with $CaCO_3$ can be divided into three stages. The first is the diffusion of H^+, followed by the contact of H^+ with $CaCO_3$, and finally, the detachment of the reaction products. Therefore, we attempt to propose that the contact between H^+ and $CaCO_3$ can be impeded by forming an adsorption film on the surface of $CaCO_3$, consequently reducing the acid−rock reaction rate.[19] The adsorption film reduces the rate of acid−rock reaction by controlling the contact between H^+ and $CaCO_3$. It differs from gelled acid essentially in that gelled acid has large molecular weight and high viscosity, it will make the hydrodynamic volume much larger than the radius of the pore throat, it will even block the channel, and it will cause secondary damage. Meanwhile, in our previous studies,[20,21] we found that the cationic acrylamide polymers based on long-chain quaternary ammonium salts adsorb on the surface of $CaCO_3$ to form an adsorption film, thereby inhibiting the contact of H^+ with $CaCO_3$. However, the adsorption force is unclear, and the thickness of the adsorption film has not been investigated further. On the other hand, the long-chain quaternary ammonium salt is arduous to degrade, which may adversely affect the improvement of reservoir permeability, especially in tight carbonate reservoirs. Therefore, we replaced it with long-chain-containing ester groups to synthesize the nonionic acrylamide polymers in this work and examined whether nonionic acrylamide polymers can also adsorb on the $CaCO_3$ surface to reduce the acid−rock reaction rate.

In this study, we selected allyl poly(ethylene glycol) (highly ethoxylated, capable of interacting with hydroxyl groups on the surface of $CaCO_3$) as the adsorption monomer,[22] octadecyl methacrylate (containing ester groups, hydrolyzable) to provide a long hydrophobic chain, and acrylamide as the main chain to synthesize the nonionic acidizing retarder AAO. The structure of AAO was characterized by Fourier transform infrared (FT-IR) spectrometry and ^1H nuclear magnetic resonance (^1H NMR). The adsorption behavior, thickness of the adsorption film, and performance in delaying the acid−rock reaction were systematically investigated for AAO. At the same time, the effect of urea on AAO adsorption capacity was discussed. The surface morphology changes of $CaCO_3$ before and after adsorption were explored by scanning electron microscopy (SEM). Finally, FT-IR was used to test the variation of AAO retard acid after 2 h of the acid−rock reaction.

2. EXPERIMENTAL SECTION

2.1. Experimental Materials. Acrylamide (AM), carbonate rocks (particles of 40 mesh and cylinders of 20.00 mm in height and 25.26 mm in diameter, industrial grade), OP-10, and ethanol (analytical grade) were purchased from Chengdu Ke Long Chemical Reagent Factory, Sichuan, China. The main component of the carbonate rocks used was $CaCO_3$, which was confirmed by X-ray diffraction (XRD). Allyl poly(ethylene glycol) (APEG-700, industrial grade) was procured from Jiangsu Hai An Petrochemical, Jiangsu, China. Octadecyl methacrylate (OM, analytical grade) was provided by Shanghai Aladdin Biochemical Technology Company, Shanghai, China. 2,2-Azobis (2-methylpropionamidine) dihydrochloride (AIBA, analytically pure) was obtained from Qu-Zhou Rui-Er-Feng Chemical, Zhejiang, China. Deionized water was homemade.

2.2. Synthesis of Polymer AAO. First, 134.64 g of deionized water and 9.42 g of OP-10 were added to a 250 mL three-necked flask and dissolved by stirring at 40 °C to obtain a clear and transparent solution. Then, 21.32 g of AM, 2.10 g of APEG-700, and 0.34 g of OM were added to the solution in sequence and stirred until completely dissolved. Next, N_2 was pumped into the solution for 0.5 h to remove the dissolved oxygen in the solution. Finally, 0.0594 g of AIBA as an initiator was added, and the reaction was polymerized at 45 °C for 6 h. After the reaction was completed, the product was chopped with scissors, washed three times with ethanol, and vacuum-dried for 1 day at 55 °C to acquire the retarder AAO. The synthetic route of AAO is shown in Scheme 1.

Scheme 1. Synthesis of AAO

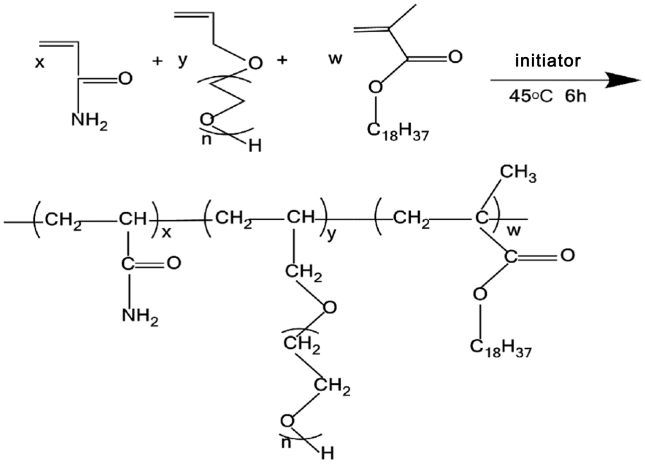

2.3. Characterizations and Measurements. *2.3.1. Structural Characterization.* The AAO powder was mixed with potassium bromide (KBr), ground, and tableted. The AAO structure was characterized by a WRF-520 Fourier transform infrared (FT-IR) spectrometer purchased from Beijing Rui Li Analytical Instruments Co., Ltd., Beijing, China. The ^1H nuclear magnetic resonance (^1H NMR) spectrum was determined for the fully dissolved 0.0020 g of AAO powder with 1 mL of D_2O using an Ascend Model 400 high-frequency NMR spectrometer (Bruker Co., Switzerland) at room temperature.

https://doi.org/10.1021/acsomega.3c03849
ACS Omega 2023, 8, 39041−39051

2.3.2. Molecular Weight Determination. AAO solution (2 mg/mL) was prepared by the mixture solution of 0.1 mol $NaNO_3$ and 0.05% NaN_3, and its molecular weight and distribution were measured using Rid-20A gel permeation chromatography (Shimadzu Co., Japan) with a flow velocity of 0.6 mL/min at 35 °C.

2.4. Performance Test of the Delaying Acid−Rock Reaction. To prepare the retard acid solutions, we dissolved 0.4, 0.6, and 0.8% (mass percent) AAO in 30 g of 20% hydrochloric acid (HCl). Meanwhile, hydrochloric acid without AAO was used as a blank sample. The effect of AAO dosage on the reaction between HCl and $CaCO_3$ was studied at 50 °C. Moreover, the reaction area of the $CaCO_3$ cylinder was fixed at 5 cm^2 by epoxy resin,[23] and a flowmeter was employed to accurately record the CO_2 volume generated at different times. Figure 1 presents the experimental device.

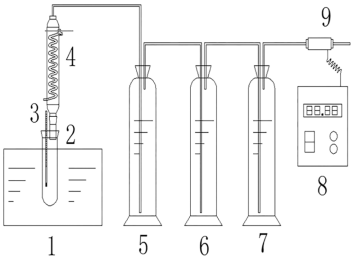

Figure 1. Experimental device for gas collection: 1, water bath; 2, reaction vessel; 3, thermometer; 4, condenser pipe; 5 and 6, water (removal of HCl); 7, $CaCl_2$ (adsorb water); 8, flowmeter; 9, flow sensor.

2.5. Adsorption Test. *2.5.1. Standard Preparation.* First, the 10,000 mg/L AAO solution was prepared by dissolving 1.0 g of AAO in 100 mL of deionized water. Then, it was diluted with deionized water at different multiples to obtain dilute solutions (100−10,000 mg/L). Finally, an ultraviolet−visible light test was performed on these dilute solutions of different concentrations. The scanning range was 200−400 nm for a UV-1800 ultraviolet spectrophotometer (Shimadzu Co., Japan).

2.5.2. Adsorption Kinetics. First, 5 g of $CaCO_3$ particles was added to a conical flask containing 100 mL of AAO solutions of various concentrations. Next, the conical flask was sealed and placed in a constant-temperature oscillating table at 30 °C for adsorption. The solution was centrifuged at 3000 rpm for 10 min after completion of adsorption. The absorbance of the centrifuged supernatant was measured by a UV-1800 ultraviolet spectrophotometer. Each absorbance was measured three times, and an average was taken. Then, the absorbance was used with the equation of the standard curve to calculate the equilibrium concentration. Finally, the adsorption capacity was calculated once every 15 min until adsorption equilibrium.[24] The formula of adsorption capacity is as follows

$$Q = \frac{(C_o - C_e)V}{m} \quad (1)$$

where Q (mg/g) is the adsorption capacity, C_o (mg/L) is the initial concentration of the AAO solution, C_e (mg/L) is the equilibrium concentration, m (5 g) is the mass of $CaCO_3$ particles, and V (100 mL) is the volume of the AAO solution.

2.6. Effect of Urea on Adsorption Capacity. The first group was operated as described in Section 2.5.2. The second group was operated under identical conditions, except for the addition of 0.5 g of urea ($CO(NH_2)_2$). The shaking time was equivalent to the adsorption equilibrium time.

2.7. X-ray Photoelectron Spectroscopy (XPS) Measurements. XPS can determine the type and content change of elements on the surface of materials. Element content scans of $CaCO_3$ before and after adsorption were performed using an ESCALAB 250Xi XPS instrument (Thermo Fisher Scientific). The thickness of the adsorption film for AAO on $CaCO_3$ was calculated using the specific empirical formula.

2.8. Scanning Electron Microscopy (SEM) Observations. SEM is a common method for observing the surface morphology of samples. The four cylinders of $CaCO_3$ were named a, b, c, and d. Among them, a was blank without being processed, b was treated with hydrochloric acid only, and c and d were treated with 0.8% AAO retard acid solution at 50 °C. After treatment, b and c were dried naturally, and d was soaked in tap water for 5 min and dried naturally. The ratio of the volume of 20% hydrochloric acid to the reaction area of $CaCO_3$ (5 cm^2) was 20:1. The apparent morphology of the above samples was examined by an EVO MA15 SEM instrument (ZEISS Co., Germany).

2.9. Variation of AAO before and after the Reaction. Gelled acid used in reservoir stimulation has the remarkable characteristics of large molecular weight and high viscosity, which often remain in the formation after the construction is completed, causing secondary damage to the reservoirs. However, ester groups degrade easily compared with other functional groups and do not cause damage to the environment. Therefore, the decomposition of 0.8% AAO retard acid before and after the acid−rock reaction at 90 °C was investigated by a Nicolet 6700 Fourier transform infrared spectrometer (Thermo Fisher Scientific).

3. RESULTS AND DISCUSSION

3.1. Characterization of AAO. Infrared spectrometry is an analytical instrument that utilizes the absorption characteristics of substances with infrared radiation of different wavelengths to identify molecular structure. The FT-IR spectra of AAO were measured by the KBr tablet method, and the result is shown in Figure 2. It could be seen that the stretching vibration peak at 3410 cm^{-1} was ascribed to − NH_2 from acrylamide, the 2912 and 2847 cm^{-1} peaks were assigned to $-CH_3$ and $-CH_2$ stretching, respectively; the 2400 cm^{-1} peak was generated by the influence of CO_2 in the air, the 1670

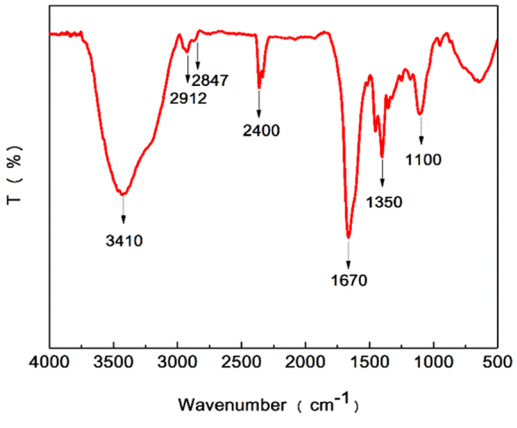

Figure 2. Infrared spectra of AAO.

https://doi.org/10.1021/acsomega.3c03849
ACS Omega 2023, 8, 39041−39051

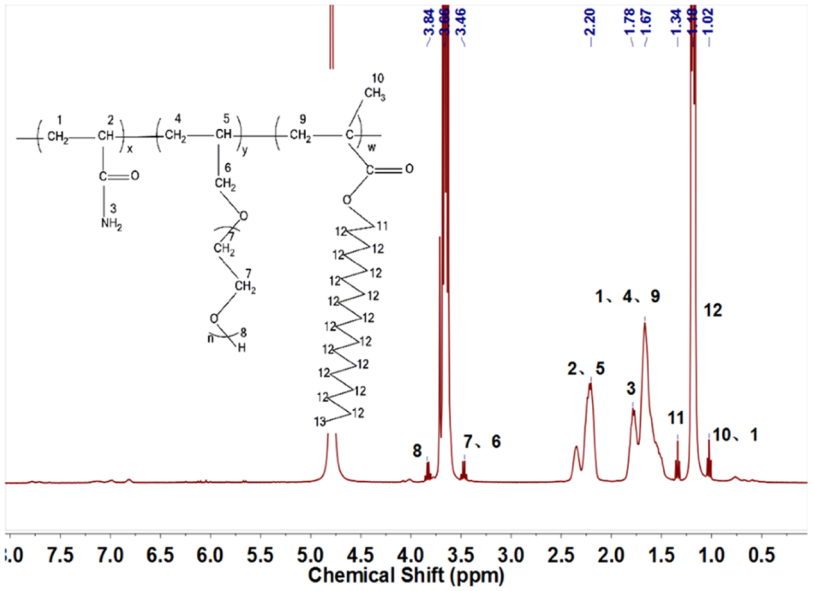

Figure 3. ^{1}H NMR spectra of AAO.

cm^{-1} peak was due to the stretching vibration of C═O in the amide group, the 1350 cm^{-1} peak was ascribed to −CO vibration in the ester group, and the 1100 cm^{-1} peak was the characteristic stretching vibration peak of −C−O−C− in allyl poly(ethylene glycol). There was no vibration peak of C═C in Figure 2, which proved that AAO was successfully synthesized.

To further verify the structure of AAO, the ^{1}H NMR test was carried out, and the result is represented in Figure 3. The chemical shifts of different hydrogens in the AAO molecule were as follows for δ (ppm): δ = 1.02 (10, 13, −CH_3), δ = 1.18 (12, −CH_2−), δ = 1.34 (11, −CH_2−), δ = 1.67 (1, 4, 9, −CH_2−), δ = 1.78 (3, −NH_2), δ = 2.20 (2, 5, −CH−), −CH_2− (6) appeared at δ = 3.46, the peak at δ = 3.66 was for −CH_2− (7) and the −OH (8) was ascribed at δ = 3.84. Thus, the ^{1}H NMR spectrum also confirmed that the AAO was prepared successfully.

Nowadays, the thickening agent used in reservoir stimulation reduces the reaction rate between acid solution and carbonate rocks due to the increase in viscosity, which means that the thickening agent possesses an outstanding feature of large molecular weight. So, determining the molecular weight of AAO is inevitable because our research focuses on adsorption rather than viscosity increase. Table 1 lists the gel permeation chromatography (GPC) test result of AAO. From Table 1, the weight-average molecular weight (M_W) and number-average molecular weight (M_n) of AAO were 891,140 and 427,474, respectively. Compared to the thickening agent with millions of M_W, AAO has a small M_W, which was conducive for quick dissolution in acid solution to prepare the retard acid. The polydispersity of AAO was 2.08, with a narrow molecular distribution.

Table 1. Molecular Weight of AAO

M_W	M_n	polydispersity (M_W/M_n)
891,140	427,474	2.08

3.2. Retard Performance of AAO. The adsorption film can effectively delay the contact between H^+ and $CaCO_3$, thereby reducing the acid−rock reaction rate. Therefore, it is necessary to explore the retard performance of AAO. First, AAO with different dosages (0.4, 0.6, and 0.8%) was added to 30 g of 20% hydrochloric acid to prepare the AAO retard acid. The reaction area of the $CaCO_3$ cylinder was fixed at 5 cm^2 by epoxy resin, and the ratio between acid and rocks was 6 g/cm^2. One group without AAO was the blank. Next, the retard performance of the AAO retard acid at 50 °C was evaluated by the experimental device shown in Figure 1.[21] The volume of CO_2 was recorded every 5 min, and the reaction rate was calculated. The results are displayed in Figure 4.

According to Figure 4a, the CO_2 generated by the reaction between different concentrations of AAO retard acid and $CaCO_3$ increased with time, the whole trend was pretty flat, and the reaction time could be up to 120 min. Meanwhile, the larger the amount of AAO, the less the CO_2 generated during the same time. As for the blank sample, the whole reaction was stopped at 45 min. The volume of CO_2 generated by the blank sample promptly increased to about 1500 mL when the reaction was carried out for 20 min. In contrast, the CO_2 produced by 0.8% AAO retard acid was less than 400 mL, and it did not exceed 800 mL at the end of the reaction, about half of that of the blank sample, which showed that the AAO retard acid had the effect of significantly prolonging the reaction time. Simultaneously, the volume of CO_2 generated in the same period gradually decreased with an increase in the AAO dosage, which implied that AAO could reduce the acid−rock reaction rate drastically. As shown in Figure 4b, various concentrations of retard acid reduced the reaction rate to a fairly low level in about 20 min and maintained it until the end of the reaction. Compared with the blank sample, the reaction rate between the 0.8% AAO retard acid and $CaCO_3$ was as low as 0.020 g/cm^2·min at 5 min, reaching about one-seventh of that of the blank sample (0.145 g/cm^2·min). The addition of AAO not only extended the reaction time from 40 to 120 to 120 min but also kept the reaction rate low throughout the entire reaction period. This may be due to the strong hydrogen bonds effect between AAO and $CaCO_3$. As a result, AAO was adsorbed on the surface of $CaCO_3$ and formed a layer of the adsorption film that hindered the contact between H^+ and

https://doi.org/10.1021/acsomega.3c03849
ACS Omega 2023, 8, 39041−39051

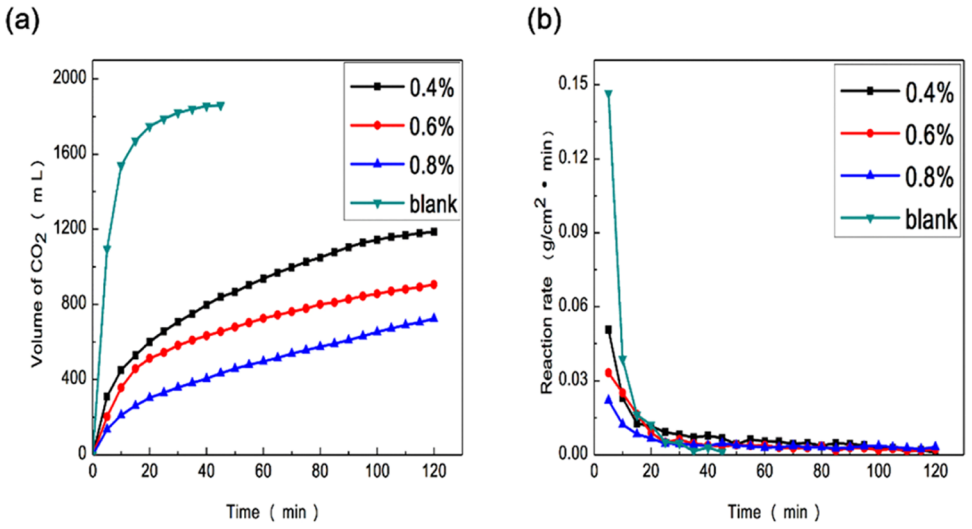

Figure 4. Effect of AAO dosage on acid−rock reaction: (a) volume of CO_2 and (b) reaction rate.

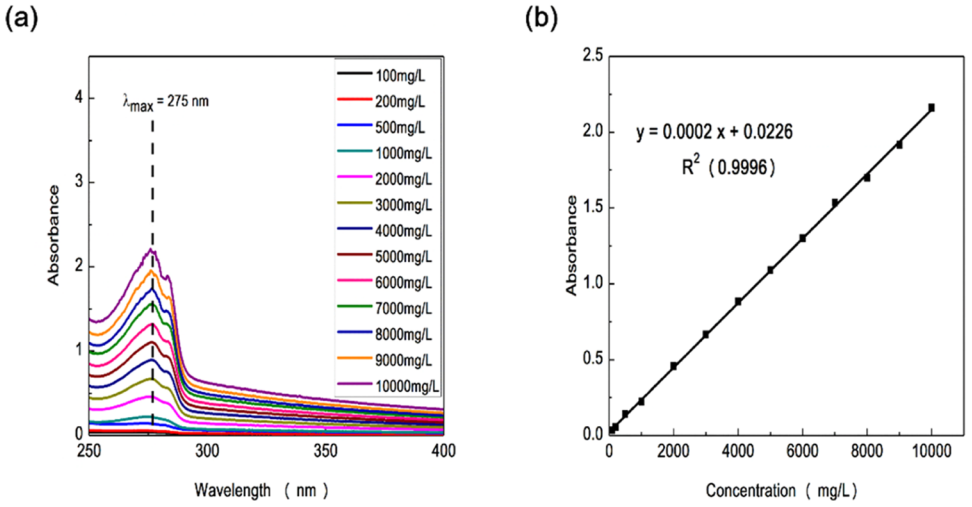

Figure 5. Spectra scanning of AAO solution: (a) UV spectra and (b) standard curve.

$CaCO_3$, resulting in a sharp decrease in the acid−rock reaction rate.

3.3. Standard Curve of AAO. At present, the adsorption capacity is determined by the concentration difference before and after adsorption. A standard curve of concentration and absorbance must be established because it is challenging to determine the concentration of the solution after adsorption directly. The concentration can be calculated in reverse by measuring the absorbance of the solution after adsorption. The ultraviolet absorption curves of AAO solution with different concentrations are shown in Figure 5. It was easy to observe that AAO had an intense absorption peak at 275 nm, as shown in Figure 5a. The absorbance of varying concentrations of AAO solution at 275 nm was fitted to obtain the standard curve. As appeared in Figure 5b, the standard curve conformed to the Lambert−Beer Law, which showed a linear relationship between absorbance and AAO concentration in the range of 0−10,000 mg/L, and the linear fitting was as high as 99.96%, signifying the high availability of this method. Thus, the standard curve could be used to determine the concentration of AAO solution after adsorption and calculate the adsorption capacity.

3.4. Adsorption Kinetics. Adsorption kinetics research is crucial for determining the adsorption mechanism and reflecting the factors that influence the sorption.[25] With the continuous advancement of kinetics research in recent decades, researchers have established a variety of kinetic models. Among them, the pseudo-first-order and pseudo-second-order kinetic models are the most widely used.[26] The mathematical expression of the model is as follows[27]

$$\ln(Q_{e,1} - Q_t) = \ln Q_{e,1} - k_1 \times t \quad (2)$$

$$\frac{t}{Q_t} = \frac{1}{Q_{e,2}}t + \frac{1}{k_2 Q_{e,2}^2} \quad (3)$$

Equations 2 and 3 are pseudo-first-order and pseudo-second-order kinetic models, respectively. $Q_{e,1}$ (mg/g) and $Q_{e,2}$ (mg/g) represent the pseudo-first-order and pseudo-second-order kinetic fitted equilibrium adsorption capacities, respectively, k_1 (min^{-1}) and k_2 (mg/g·min) denote the pseudo-first-order kinetic and pseudo-second-order kinetic adsorption rate constants, respectively, and Q_t (mg/g) is the adsorption capacity at any time. Figure 6 depicts the relationship between

https://doi.org/10.1021/acsomega.3c03849
ACS Omega 2023, 8, 39041−39051

the AAO adsorption capacity and time at various initial concentrations from 1000 to 5000 mg/L.

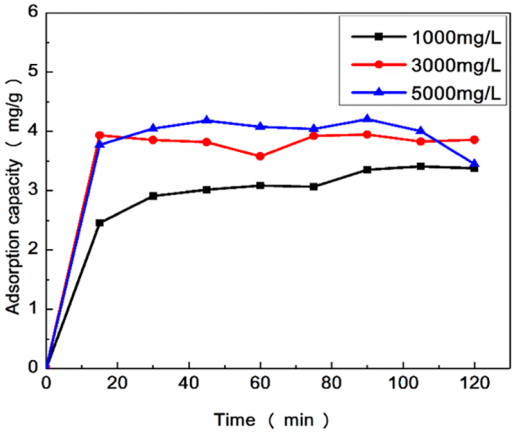

Figure 6. Effect of concentration on the adsorption of AAO on $CaCO_3$.

As observed from Figure 6, the adsorption capacity of AAO on $CaCO_3$ increased with time, and the whole process could be divided into two parts: the adsorption process was rapid, and the adsorption capacity increased sharply within the initial 20 min; this was highly consistent with the results presented in Figure 4 (the reaction rate reduced to a pretty low level in about 20 min). After 20 min, the adsorption capacity increased slowly and gradually reached equilibrium. Simultaneously, an increase in AAO concentration was found to be positively related to adsorption capacity. This was because an increase in concentration increases the chance of contact between AAO and the surface of $CaCO_3$, resulting in a larger adsorption capacity.

Figure 7 displays the pseudo-first-order and pseudo-second-order kinetic fitted results separately. Detailed data are shown in Tables 2 and 3.

From Tables 2 and 3, the correlation coefficient (R^2) of the pseudo-second-order kinetic equation was higher than that of the pseudo-first-order kinetic equation at 30 °C. Meanwhile, the equilibrium adsorption capacity of the pseudo-second-order kinetic equation was closer to the true equilibrium adsorption capacity. Thus, the pseudo-second-order kinetic model better reflected the kinetic behavior of AAO on $CaCO_3$. Compared with 1000 and 5000 mg/L, when the initial concentration was 3000 mg/L, the fitted equilibrium adsorption capacity was almost the same as the true adsorption capacity, and the pseudo-second-order kinetic adsorption rate constant k_2 was the largest, which showed that the internal diffusion of $CaCO_3$ particles caused by the concentration difference of AAO played a crucial role in the adsorption rate.[28]

3.5. Adsorption Force for AAO on $CaCO_3$. Adsorption force induces the occurrence of adsorption behavior, which is also related to the interaction between the adsorbent and the adsorbate and affected by the environment. At present, adsorption forces are mainly divided into physical adsorption, such as hydrogen bonding,[29,30] and chemical adsorption, such as ion exchange[31] and electrostatic interaction.[32] In this study, the adsorbate AAO is a nonionic polymer that does not ionize any charged ions in aqueous solution. Therefore, we speculate that the adsorption force between AAO and $CaCO_3$ particles may be hydrogen bonding. In the next, we explored the effect of urea on adsorption capacity of AAO to verify our proposed conjecture, and the result is shown in Figure 8.

The molecular structure of urea has a high degree of spatial symmetry and contains a large number of amino groups. Amino groups have strong electronegativity and can easily form intermolecular hydrogen bonds with other functional groups. Hence, it is also known as a hydrogen bond breaker.[33] It can preferentially form hydrogen bonds with water and polymers, thereby effectively preventing the formation of hydrogen bonds between the polymer in solution and the solid particle surface.[34] Figure 8 shows that the adsorption capacity increased slowly with the initial concentration from 1000 to 5000 mg/L, while it increased sharply from 5000 to 8000 mg/L; the whole stage showed an L shape. After the concentration exceeded 5000 mg/L, part of AAO was adsorbed and arranged on the surface of $CaCO_3$, and the other followed in the form of overlapping so that the adsorption capacity increased sharply. Furthermore, the adsorption capacities of different initial concentrations showed a significant decrease after urea addition, which indicated that the addition of urea reduced the number of AAO molecules adsorbed on the surface of

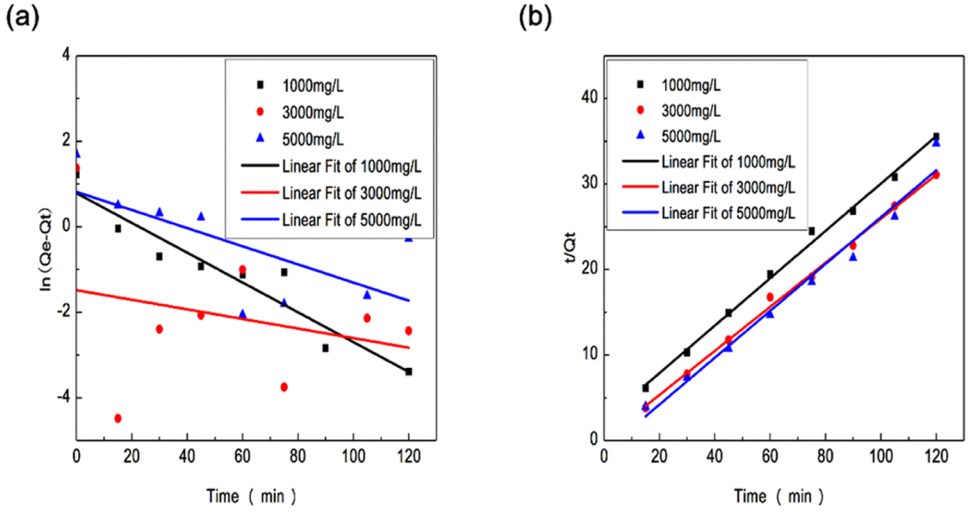

Figure 7. Kinetic fits for adsorption of AAO on $CaCO_3$: (a) pseudo-first-order and (b) pseudo-second-order.

https://doi.org/10.1021/acsomega.3c03849
ACS Omega 2023, 8, 39041−39051

Table 2. Pseudo-First-Order Kinetic Parameters

initial concentration (mg/L)	Q_e (mg/g)	kinetic equation	R_1^2	$Q_{e,1}$ (mg/g)	k_1 (min^{-1})
1000	2.7416	$y = -0.0348x + 0.7871$	0.8938	2.1969	0.0348
3000	3.4169	$y = -0.0112x - 1.4837$	0.0831	0.2268	0.0112
5000	3.5325	$y = -0.0212x + 0.8176$	0.3663	2.2651	0.0212

Table 3. Pseudo-Second-Order Kinetic Parameters

initial concentration (mg/L)	Q_e (mg/g)	kinetic equation	R_2^2	$Q_{e,2}$ (mg/g)	k_2 (g/mg·min)
1000	2.7416	$y = 0.2771x + 2.3447$	0.9953	3.6083	0.0328
3000	3.4169	$y = 0.2576x + 0.1801$	0.9966	3.8815	0.3686
5000	3.5325	$y = 0.2246x + 3.7238$	0.8924	4.4526	0.0135

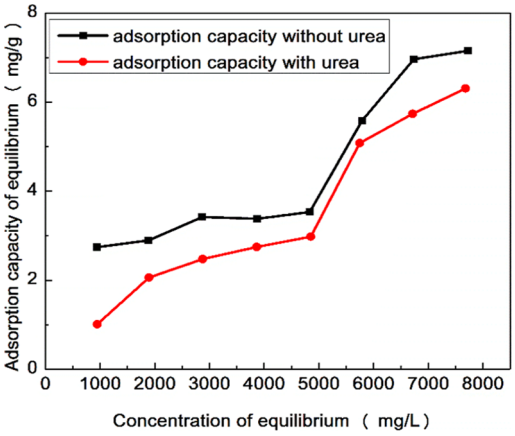

Figure 8. Effect of urea on the adsorption capacity of AAO.

$CaCO_3$. It demonstrated that the adsorption force between AAO and $CaCO_3$ is hydrogen bonding. Because APEG contains numerous ethylene oxide groups, and the oxygen atoms in the ethylene oxide groups can interact with hydroxyl groups on the surface of $CaCO_3$ to form hydrogen bonds.[23] After urea was added, urea had the priority to form hydrogen bonds between water and AAO molecules, which destroyed the original hydrogen bonds between AAO molecules and $CaCO_3$ particles. As a result, the adsorption capacity of AAO on the surface of $CaCO_3$ decreased.

3.6. Thickness of the Adsorption Film of AAO. X-rays can excite electrons in the outermost layer of an atom, causing them to be free. The energy change of free electrons passing through the adsorption layer can be used to approximate the adsorption layer thickness. The energy change decreases exponentially, and the mathematical expression is[35]

$$dI = -I_0 \frac{db}{\lambda(E_k)} \tag{4}$$

where I_0 is the initial photoelectron intensity, db (nm) is the penetration distance, dI is the loss intensity, and $\lambda(E_k)$ is a constant that is related to the photoelectron kinetic energy E_k; E_k is referred to as the average escape depth. Under the boundary condition ($b = 0$, $I = I_0$), eq 4 is integrated, resulting in the following equation

$$I_b = I_0 e^{-b/\lambda(E_k)} \tag{5}$$

Based on a large amount of experimental data, the empirical formula suitable for inorganic compounds as adsorbents has been summarized by researchers

$$\lambda(E_k) = 2170E_k^{-2} + 0.72(\alpha E_k)^{0.5} \tag{6}$$

$$\alpha^3 = \frac{10^{24}M}{\rho m N} \tag{7}$$

$$h\nu = E_k + E_b \tag{8}$$

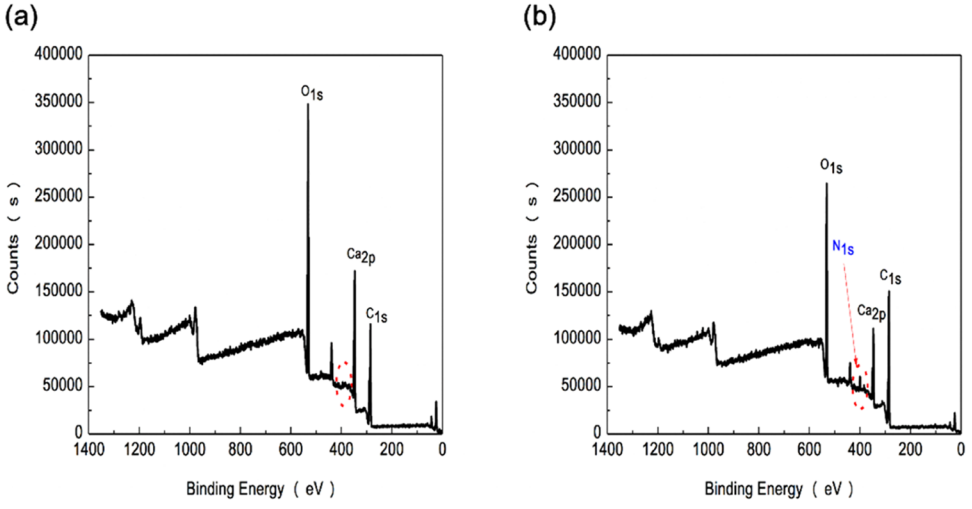

Figure 9. Scanning diagram of XPS for $CaCO_3$: (a) before adsorption and (b) after adsorption.

https://doi.org/10.1021/acsomega.3c03849
ACS Omega 2023, 8, 39041−39051

where hv (1486.6 eV) represents the light source energy, E_k (eV) is the photoelectron kinetic energy, E_b (347.1 eV) is the binding energy of $Ca_{2p(3/2)}$ in pure $CaCO_3$, α (nm) is the monatomic layer thickness, M (100.09 g/mol) is the relative molecular mass of $CaCO_3$, m (1) is the number of Ca atoms in a molecule of $CaCO_3$, ρ (2930 kg/m^3) is the density of $CaCO_3$, and N (6.02×10^{23}) is the Avogadro constant.

The $CaCO_3$ particles before and after adsorption were detected by an ESCALAB 250Xi X-ray photoelectron spectroscopy (XPS) instrument. The results are shown in Figure 9 and Tables 4 and 5.

Table 4. Elements of $CaCO_3$ before Adsorption

name	peak	fwhm (eV)	area	atomic (%)
O 1s	530.84	3.26	965,348.08	41.38
Ca 2p	346.13	3.07	559,603.75	10.50
C 1s	284.21	3.00	442,120.37	48.12

Table 5. Elements of $CaCO_3$ after Adsorption

name	peak	fwhm (eV)	area	atomic (%)
O 1s	530.87	3.57	759,128.22	31.88
C 1s	284.31	3.23	555,862.44	59.28
Ca 2p	346.00	3.14	305,362.18	5.61
N 1s	398.87	2.94	48,007.27	3.23

As indicated in Figure 9a, the scanning diagram of XPS elements for $CaCO_3$ particles before adsorption only contained three elements of Ca, C, and O, which certified the high purity of $CaCO_3$ that had no other impurities. In contrast, four elements were tested successfully by XPS after the adsorption of AAO on the surface of $CaCO_3$, as shown in Figure 9b. Thus, we hold on to the view that the additional N element marked by the red dotted circle in Figure 9b came from the amino group ($-NH_2$) in the AAO, which demonstrated that the AAO adsorbed on $CaCO_3$ from the microscopic view and the AAO played a crucial role in delaying the acid−rock reaction.

Next, we researched this film formed by the adsorption of AAO on $CaCO_3$. The AAO molecule did not contain the element Ca, while $CaCO_3$ did. Theoretically, the strength of the element would be reduced due to the existence of the adsorbed film during the XPS test. So, we regarded Ca as the characteristic element. By studying the strength changes of Ca before and after adsorption and using the empirical formula, the thickness of the adsorption layer can be obtained. The results from Tables 4 and 5 exhibited that the intensity of Ca decreased from 559,603.75 (I_0) before adsorption to 305,362.18 (I_b) after adsorption. This was explained by the adsorption of AAO being equivalent to covering the surface of $CaCO_3$ with a film, which reduced the number of Ca atoms colliding with photoelectrons and resulted in a decrease in the intensity of Ca detected after adsorption. Finally, it was easy to calculate that E_k, α, $\lambda(E_k)$, and b were 1139.5 eV, 0.3842, 15.0653, and 9.125 nm based on eqs 5−8, respectively. Therefore, the adsorption film thickness of AAO on $CaCO_3$ particles was approximately 9.125 nm.

3.7. Observation of the Morphology of $CaCO_3$. The apparent morphologies of the treated $CaCO_3$ via different methods were observed by a ZEISS EVO MA15 scanning electron microscopy (SEM) instrument. In this way, we could

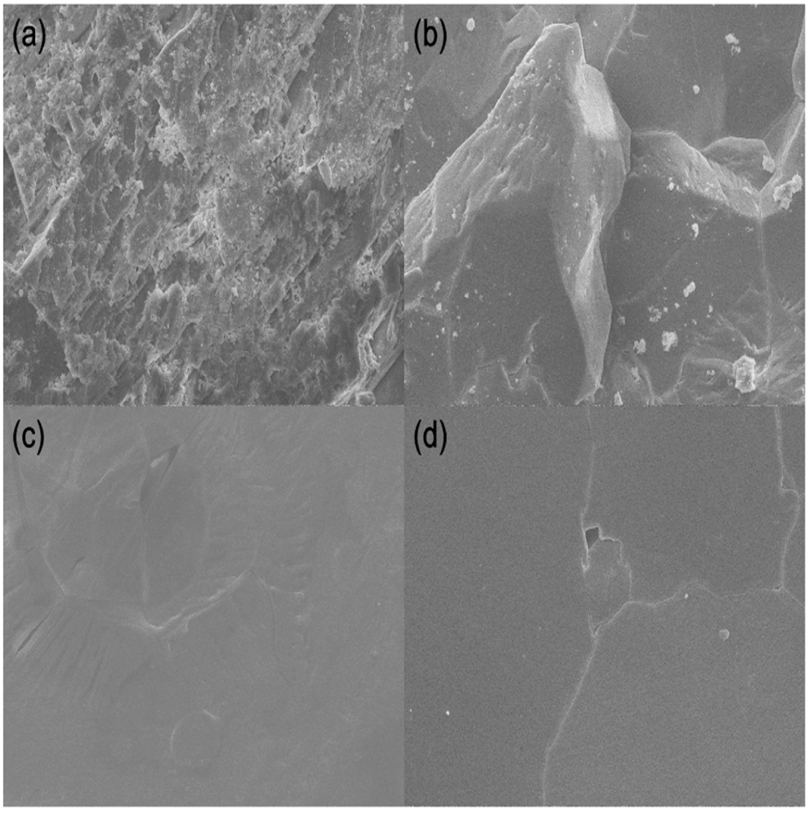

Figure 10. SEM images of different $CaCO_3$ samples (500 times): (a) without treatment, (b) treated with 20% hydrochloric acid, (c) treated with 0.8% AAO retard acid, and (d) treated with 0.8% AAO retard acid and soaked in tap water.

https://doi.org/10.1021/acsomega.3c03849
ACS Omega 2023, 8, 39041−39051

better understand the mechanism of AAO delaying the acid−rock reaction. The results are shown in Figure 10.

As presented in Figure 10a, the surface of untreated $CaCO_3$ was extremely rough, and some small rock particles existed, which was natural. The surface of $CaCO_3$ treated with 20% hydrochloric acid was crisscrossed with ravines, and the etching morphology was very irregular, as shown in Figure 10b. This was the result of the violent reaction of hydrogen ions with the rock surface, which we called irregular etching. Surprisingly, the surface of $CaCO_3$ treated with 0.8% AAO retard acid became pretty smooth and flat, and even a slightly transparent dense film could be seen in Figure 10c, which was quite different from the results shown in Figure 10a,b. The film contributed to delaying the contact of H^+ with $CaCO_3$, thereby reducing the progress of the acid−rock reaction. Water flooding is required after acidification to enhance oil and gas recovery. As shown in Figure 10d, this film desorbed gradually after immersion in tap water, leaving many microchannels for the free flow of oil and gas, and may not cause secondary damage to the reservoirs. Finally, compared to gelled acid that relied on extreme viscosity to reduce the rate of the acid−rock reaction, we measured the viscosity of 0.8% AAO retard acid by a ZNN-D6 six-speed rotational viscometer at 170 s^{-1} for 25 °C. The viscosity of most commercial gelled acid solutions reported in the literature[21] was about 30 mPa·s, while the viscosity of 0.8% AAO retard acid was only 15 mPa·s. It was also demonstrated that AAO delayed the acid−rock reaction through the adsorption film rather than increasing the viscosity of the acid solution. Meanwhile, the lower viscosity is beneficial to the smooth flowback of the retard acid and the small possibility of retention in reservoirs and will not cause secondary damage to the formation.

3.8. Variation of AAO before and after the Reaction.

Previous research by our group has confirmed that the introduction of a long-chain quaternary ammonium salt into an acidizing retarder can significantly enhance the retard performance.[36] However, such retarders take more time to degrade due to the stability of the alkyl chain. If they remained, they will contaminate the reservoirs. Therefore, we synthesized a nonionic acidizing retarder by using long-chain esters instead of long-chain quaternary ammonium salts and studied its decomposition after the acid−rock reaction. The 0.8% AAO retard acid solution before (0 h) and after (2 h) the reaction was dropped on the pressed potassium bromide sheet and tested by a Thermo Fisher Nicolet 6700 Fourier transform infrared spectrometer. The result is shown in Figure 11.

It is well known that ester groups can be hydrolyzed under the conditions of an acidic environment. Compared to the blue ellipse in Figure 11, the absorption vibration peak at 1720 cm^{-1} from C═O of the ester groups had been shifted to 1650 cm^{-1} after 2 h of the acid−rock reaction, whereas the 1650 cm^{-1} peak belonged to the vibration absorption peak of C═O in the carboxylic groups. The ether bond at 1180 cm^{-1} was also broken. By querying the standard infrared spectrum of $CaCl_2$, it was observed that the 2150 cm^{-1} peak was the absorption peak of byproduct $CaCl_2$ in the acid−rock reaction process. The above results showed that the ester groups in AAO had been hydrolyzed into carboxyl groups, the product generated by hydrolysis would desorb from the rock surface gradually, there were no large residues, and minor secondary damage occurred to the reservoirs.

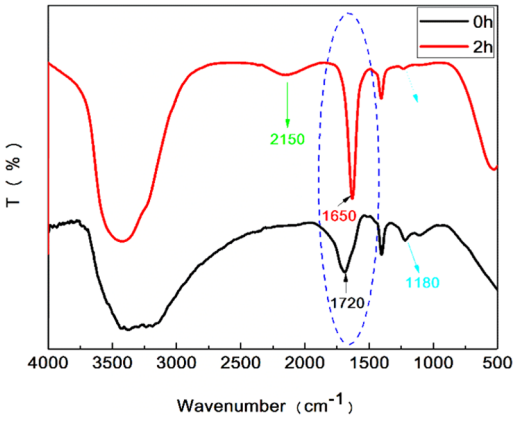

Figure 11. FT-IR spectra of AAO retard acid before and after the reaction.

4. CONCLUSIONS

Nonionic acidizing retarder AAO was prepared through emulsion polymerization using acrylamide (AM), allyl poly(ethylene glycol) (APEG), and octadecyl methacrylate (OM) as raw materials. The reaction time between the 0.8% AAO retard acid and $CaCO_3$ could be up to 120 min at 50 °C, whereas the blank (without AAO) ended at 45 min. The adsorption process of AAO on $CaCO_3$ matched the pseudo-second-order kinetic model. Furthermore, the adsorption film thickness of AAO was 9.125 nm, and the hydrogen bonding was the adsorption force between AAO and $CaCO_3$. SEM was used to successfully detect a smooth and dense film existing on the surface of $CaCO_3$. At last, the ester groups in AAO were hydrolyzed into carboxyl groups after 2 h of the acid−rock reaction, which reduced the retention in reservoirs and had little damage to the reservoirs. The above results illustrated that AAO had a tremendous performance in reducing the acid−rock reaction rate and had a specific application value in reservoir stimulation.

AUTHOR INFORMATION

Corresponding Authors

Hongping Quan − *College of Chemistry and Chemical Engineering, Southwest Petroleum University, Chengdu 610500, P. R. China; Oil & Gas Field Applied Chemistry Key Laboratory of Sichuan Province, Chengdu 610500, P. R. China;* orcid.org/0000-0001-5277-7477; Email: 59183228@qq.com

Zhiyu Huang − *College of Chemistry and Chemical Engineering, Southwest Petroleum University, Chengdu 610500, P. R. China; Oil & Gas Field Applied Chemistry Key Laboratory of Sichuan Province, Chengdu 610500, P. R. China;* orcid.org/0000-0002-9115-5571; Email: zyhuang3019@163.com

Authors

Zhonghao Chen − *College of Chemistry and Chemical Engineering, Southwest Petroleum University, Chengdu 610500, P. R. China; Oil & Gas Field Applied Chemistry Key Laboratory of Sichuan Province, Chengdu 610500, P. R. China*

Yang Wu − *College of Chemistry and Chemical Engineering, Southwest Petroleum University, Chengdu 610500, P. R. China; Oil & Gas Field Applied Chemistry Key Laboratory of Sichuan Province, Chengdu 610500, P. R. China*

https://doi.org/10.1021/acsomega.3c03849
ACS Omega 2023, 8, 39041−39051

Complete contact information is available at:
https://pubs.acs.org/10.1021/acsomega.3c03849

Notes

The authors declare no competing financial interest.

■ ACKNOWLEDGMENTS

This work was supported by the National Natural Science Foundation of China (No. 51604229), the Opening Project of the Oil & Gas Field Applied Chemistry Key Laboratory of Sichuan Province (YQKF201401, YQKF202001), and the Sichuan Science and Technology Plan Project (No. 2019YJ0315).

■ REFERENCES

(1) Zeng, H.; Zou, F. L.; Horvath-Szabo, G.; Andersen, S. Effects of brine composition on the adsorption of benzoic acid on calcium carbonate. *Energy Fuels* **2012**, *26*, 4321−4327.
(2) Ahmadi, M. A.; Shadizadeh, S. R. Experimental investigation of adsorption of a new nonionic surfactant on carbonate minerals. *Fuel* **2013**, *104*, 462−467.
(3) Ahmadi, M. A.; Shadizadeh, S. R. Adsorption of novel nonionic surfactant and particles mixture in carbonates: enhanced oil recovery implication. *Energy Fuels* **2012**, *26*, 4655−4663.
(4) Fletcher, P. D. I.; Savory, L. D.; Woods, F.; Clarke, A.; Howe, A. M. Model study of enhanced oil recovery by flooding with aqueous surfactant solution and comparison with theory. *Langmuir* **2015**, *31*, 3076−3085.
(5) Lucas, C. R. S.; Neyra, J. R.; Araújo, E. A.; Silva, D. N. N.; Lima, M. A.; Miranda Ribeiro, D. A.; Pandava Aum, P. T. Carbonate acidizing − A review on influencing parameters of wormholes formation. *J. Pet. Sci. Eng.* **2023**, *220*, No. 111168.
(6) Shen, X.; Wang, S. B.; Guo, J. C.; Chen, F. H.; Xu, B. W.; Wang, Z.; Liu, Y. X. Effect of carbon chain lengths of cationic surfactant on inhibition rate of acid-rock reaction. *J. Pet. Sci. Eng.* **2021**, *196*, No. 107793.
(7) de Oliveira Wanderley Neto, A.; da Silva, D. C.; Arruda, G. M.; da Hora, L. F.; Rodrigues, M. A. F. Chemical study of the application of nonionic surfactants nonylphenol in delaying the acidizing reaction of carbonate matrices. *J. Dispersion Sci. Technol.* **2022**, *43*, 1901−1908.
(8) Mustafa, A.; Aly, M.; Aljawad, M. S.; Dvorkin, J.; Solling, T.; Sultan, A. A green and efficient acid system for carbonate reservoir stimulation. *J. Dispersion Sci. Technol.* **2021**, *205*, No. 108974.
(9) Jora, M. Z.; de Souza, R. N.; Lucas-Oliveira, E.; Speglich, C.; Bonagamba, T. J.; Sabadini, E. Static acid dissolution of carbonate outcrops investigated by ^{1}H NMR and X-ray tomography. *J. Dispersion Sci. Technol.* **2021**, *207*, No. 109124.
(10) Mehrjoo, H.; Norouzi-Apourvar, S.; Jalalifar, H.; Shajari, M. Experimental study and modeling of final fracture conductivity during acid fracturing. *J. Pet. Sci. Eng.* **2022**, *208*, No. 109192.
(11) Martyushev, D. A.; Govindarajan, S. K.; Li, Y. W.; Yang, Y. F. Experimental study of the influence of the content of calcite and dolomite in the rock on the efficiency of acid treatment. *J. Pet. Sci. Eng.* **2022**, *208*, No. 109770.
(12) Aum, P. T. P.; Aum, Y. K. P. G.; Araújo, E. A.; Cavalcante, L. A.; Silva, D. N. N.; Lucas, C. R. S.; Dantas, T. N. C. Evaluation of oil-in-water microemulsion base ethoxylated surfactant under acid conditions. *Fuel* **2021**, *290*, No. 120045.
(13) Yan, Y. L.; Xi, Q.; Una, C. C.; He, B. C.; Wu, C. S.; Dou, L. L. A novel acidizing technology in carbonate reservoir: in-Situ formation of CO_2 foamed acid and its self-diversion. *Colloids Surf., A* **2019**, *580*, No. 123787.
(14) Mao, J. C.; Wang, D. L.; Yang, X. J.; Zhang, Z. Y.; Yang, B.; Zhang, C. Adsorption of surfactant on stratum rocks: exploration of low adsorption surfactants for reservoir stimulation. *J. Taiwan Inst. Chem. Eng.* **2019**, *95*, 424−431.
(15) Gomaa, A. M.; Nasr-El-Din, H. A. Effect of elastic properties on the propagation of gelled and in-situ gelled acids in carbonate cores. *J. Pet. Sci. Eng.* **2015**, *127*, 101−108.
(16) Nourafkan, E.; Hu, Z. L.; Wen, D. S. Controlled delivery and release of surfactant for enhanced oil recovery by nanodroplets. *Fuel* **2018**, *218*, 396−405.
(17) Kalam, S.; Abu-Khamsin, S. A.; Patil, S.; Mahmoud, M.; Kamal, M. S.; Murtaza, M.; Mohanty, K. K. Adsorption reduction of a gemini surfactant on carbonate rocks using formic acid: static and dynamic conditions. *Fuel* **2023**, *345*, No. 128166.
(18) Kesarwani, H.; Sharma, S.; Mandal, A. Application of Novel Colloidal Silica Nanoparticles in the Reduction of Adsorption of Surfactant and Improvement of Oil Recovery Using Surfactant Polymer Flooding. *ACS Omega* **2021**, *6*, 11327−11339.
(19) Zhao, F.; Wang, S. B.; Shen, X.; Guo, J. C.; Liu, Y. X. Study on mechanism of gemini surfactant inhibiting acid rock reaction rate. *Colloids Surf., A* **2019**, *578*, No. 123629.
(20) Quan, H. P.; Chen, Z. H.; Wu, Y.; Li, Z. K. Adsorption behavior of the copolymer AM/DMC/APEG/DMAAC-16 on a carbonate rock and its application for acidizing. *RSC Adv.* **2017**, *7*, 31771−31778.
(21) Quan, H. P.; Lu, Q. Y.; Chen, Z. H.; Huang, Z. Y.; Jiang, Q. Y. Adsorption-desorption behavior of the hydrophobically associating copolymer AM/APEG/C-18/SSS. *RSC Adv.* **2019**, *9*, 12300−12309.
(22) Jian, G.; Puerto, M. C.; Wehowsky, A.; Dong, P. F.; Johnston, K. P.; Hirasaki, G. J.; Biswal, S. L. Static adsorption of an ethoxylated nonionic surfactant on carbonate minerals. *Langmuir* **2016**, *32*, 10244−10252.
(23) Quan, H. P.; Li, H.; Huang, Z. Y.; Dai, S. S.; Jiang, J. F. Copolymer MCJS as a retarder of the acid-rock reaction speed for the stimulation of deep carbonate reservoirs. *J. Appl. Polym. Sci.* **2015**, *132*, No. 41471.
(24) Zhu, L.; Yang, H.; He, Y. Sodium dodecyl sulfate assisted synthesis hydroxyapatite for effective adsorption of methylene blue. *J. Dispersion Sci. Technol.* **2023**, *44*, 1618−1627.
(25) Liu, Y. J.; Qi, R. X.; Ge, Z. S.; Zhang, Y. Q.; Jing, L. Y.; Li, M. N-doping copolymer derived hierarchical micro/mesoporous carbon:-Pore regulation of melamine and fabulous adsorption performances. *J. Taiwan Inst. Chem. Eng.* **2021**, *120*, 236−245.
(26) Ahmadi, M. A.; Zendehboudi, S.; Shafiei, A.; James, L. Nonionic surfactant for enhanced oil recovery from carbonates: adsorption kinetics and equilibrium. *Ind. Eng. Chem. Res.* **2012**, *51*, 9894−9905.
(27) Liang, H.; Zou, C. J. Adsorption of naphthenic acids from oil sand process-affected water with water-insoluble poly(beta-cyclodextrin-citric acid). *Can. J. Chem. Eng.* **2019**, *97*, 1894−1902.
(28) Xue, S.; Tu, B. Y.; Li, Z. H.; Ma, X. Y.; Xu, Y. Q.; Li, M. H.; Fang, C. X.; Tao, H. S. Enhanced adsorption of Rhodamine B over Zoysia sinica Hance-based carbon activated by amminium chloride and sodium hydroxide treatments. *Colloids Surf., A* **2021**, *618*, No. 126489.
(29) Striolo, A. Studying surfactants adsorption on heterogeneous substrates. *Curr. Opin. Chem. Eng.* **2019**, *23*, 115−122.
(30) Li, P. W.; Zhao, T.; Zhao, Z. H.; Tang, H. X.; Feng, W. S.; Zhang, Z. J. Biochar Derived from Chinese Herb Medicine Residues for Rhodamine B Dye Adsorption. *ACS Omega* **2023**, *8*, 4813−4825.
(31) Altman, R. M.; Richmond, G. L. Coming to Order: Adsorption and structure of nonionic polymer at the oil/water interface as influenced by cationic and anionic surfactants. *Langmuir* **2020**, *36*, 1975−1984.
(32) Miao, J. C.; Xing, L.; Ouyang, J. Y.; Li, Z. B.; Wang, X. J. Adsorption Properties of Anionic Dyes on Quaternized Microcrystalline Cellulose. *ACS Omega* **2023**, *8*, 5617−5624.
(33) Wang, S. B.; Chen, F. H.; Guo, J. C.; Li, Y.; Zhao, F.; Zhou, S. Y. Adsorption damage of hydroxypropyl guar gum to porous media composed of quartz. *J. Pet. Sci. Eng.* **2019**, *182*, No. 106379.
(34) Das, A.; Mukhopadhyay, C. Atomistic mechanism of protein denaturation by urea. *J. Phys. Chem. B* **2008**, *112*, 7903−7908.

(35) Hu, W. *Study on the Adsorption Performance of Lignosulfonates on Surface of Solid Particle*; South China University of Technology, 2010.
(36) Quan, H. P.; Zhen, X. L.; Lu, Q. Y.; Wang, L. Y.; Jiang, S. L. The effect of hydrophobic chains on retarding performance of retarding acids. *RSC Adv.* **2022**, *12*, 9077−9086.

https://doi.org/10.1021/acsomega.3c03849
ACS Omega 2023, 8, 39041−39051